Surface damage mechanism of monocrystalline Si under mechanical loading

Qingliang Zhao[1], Quanli Zhang[1,2,3], Suet To[2], Bing Guo[1]

1.-Centre for Precision Engineering, School of Mechatronics Engineering, Harbin Institute of Technology, Harbin, 150001, China. 2.-State Key Laboratory of Ultra-precision Machining Technology, The Hong Kong Polytechnic University, Hong Kong, China. 3.-E-mail: zhangql606@163.com, TEL: +86-451 8640 2683, FAX: +86-451 8641 5244

Single point diamond scratching and nanoindentation on monocrystalline silicon wafer were performed to investigate the surface damage mechanism of Si under the contact loading. The results showed that three typical stages of material removal appeared during the dynamic scratching, and the chemical reaction of Si with the diamond indenter and oxygen under the high temperature occurred. In addition, the Raman spectra of the varied points in the scratching groove indicated that the Si-I to β-Sn structure (Si-II) and the following β-Sn structure (Si-II) to amorphous Si transformation appeared under the rapid loading/unloading condition of the diamond grit, and the volume change induced by the phase transformation resulted in the critical depth (ductile-brittle transition) of cut (~60±15 nm) to be much lower than the theoretical calculated results (~387 nm). Moreover, it also led to the abnormal load-displacement curves of the nanoindentation tests, resulting in the appearance of elbow and pop-out effect (~270 nm at 20 s, 50 mN), which was closely dependent on the loading/unloading conditions. In summary, phase transformation of Si prompted the surface deformation and fracture under both static and dynamic mechanical loadings.

Keywords: Contact loading; Ductile-brittle transition; Oxidation; Fracture; Phase transformation

INTRODUCTION

As a fundamental material in the electronic and photovoltaic fields, fabrication and processing of monocrystalline silicon devices has been widely investigated [1-5], and the surface quality of the Si devices obtained played a dominant role on the performance, such as conductivity, stability and reliability [6, 7], especially for the use of thinner silicon cells (<150 μm). For instance, the stress and fracture for the silicon cells could immediately reduce the module efficiency and result in the premature aging of the entire package [6] Therefore, much attention has been paid to the damage induced during the machining and processing stage, such as the phase transformation under high pressure (HPPT) [4, 8-16], as well as the stress state of the interconnects between the Si cell module and the Cu ribbon [17, 18]

Previous studies have shown that there are twelve different crystal structures for Si, and the hydrostatic pressure could cause the transformation between them [6, 9, 10, 14, 15]. More specifically, the diamond cubic Si (Si-I) firstly transforms to be the metallic Si-II phase (β-Sn structure) under the pressure of ~12 GPa, and a volume reduction of 22% accompanied [12, 13]. A further rise of the pressure promotes the subsequent transformation into Si-XI, Si-V, Si-VI, Si-VII and Si-X [9, 13, 19] During the unloading stage, some other structures could form depending on the pressure release conditions. Typically, the rapid unloading leads to the formation of amorphous Si, while the slow unloading results in the transformation from β-Sn structure to R8 structure (Si-XII) which further transforms to Si-III [20]. Obvious volume expansion occurs during this stage, as the densities of both amorphous Si and Si-XII/Si-III are lower than Si-II. Therefore, the volume change caused by the phase transformation of Si contributes to the abnormal loading-displacement curve during nanoindentation, that is, the elbow or pop-out appears depending on the volume change induced by the varied loading/unloading conditions. It is now well established that the abnormal curve can be induced by the phase transformation of Si [15, 21, 22]. To achieve nanometric surface finish on Si workpiece by ultra-precision technologies, ductile material removal mode is thought to be a prerequisite [4, 23]. However, during the machining processes, phase transformation of Si was always inevitable if the strain rate was taken into consideration [4, 16, 24]. Therefore, the measurement of the stress by synchrotron X-ray microdiffraction [6, 7, 17, 25, 26], the characterization of the phase structure by Raman spectroscopy [4, 27] and the investigation by the load-controlled nanoindentation have been widely performed [13, 15] and these techniques are proposed as effective approaches in investigating the damage mechanism of monocrystalline Si devices.

In addition, considering the fact that the temperature change dramatically in the contact zone between the workpiece and the diamond tool, other problem could accompany with the melting and phase transformation of Si, such as oxidation and recrystallization [16, 28, 29]. For single point diamond scratching or plunge cutting, previous studies seem to focus on the high pressure induced phase transformation or the critical depth of cut to realize ductile material removal of Si separately [16, 24, 30], while the phase transformation induced change to the critical cutting depth has been rarely investigated.

In the present work, we aims to study the impact of the phase transformation on the critical depth of cut during the diamond scratching of Si and the abnormal loading/unloading curves during nanoindentation tests, which could provide a basic knowledge of the machining induced surface damage and material removal mode in ultra-precision machining of metastable semiconductors. In addition, the chemical reaction between Si and the diamond grit and oxygen is also characterized and analyzed. The materials and experiments are given in the "EXPERIMENTAL" section of this paper. The damage mechanism of monocrystalline Si and the impact of phase transformation on the critical depth of cut during diamond scratching and the abnormal curves during nanoindentation tests are discussed in the section of "RESULTS AND DISCUSSION". Finally, the main conclusion are summarized in the "CONCLUSION" section.

EXPERIMENTAL

Commercially available monocrystalline silicon wafer N-Si<100> (Top Vendor Science & Technology Co., Ltd. China) with a size of 20×20 mm^2 was used as the workpiece. The surface finish (arithmetic mean deviation of the profile, R_a) of the Si wafer is measured to be $R_a \leq 0.5$ nm, and the total indication reading (TIR) of the Φ100 mm wafer reaches $TIR < 3$ μm. Dry scratching test was performed on a precision grinding machine MUGK7120X5 (Hangzhou Machine Tool Group Co., Ltd., China). The diamond indenter was fixed to a steel disc and the diameter of the sharp point was about 230 mm with a rotation speed of 50 revolutions per minute (RPM). The experimental setup was illustrated in Fig.1 (a) and a typical scratching groove was shown in Fig.1 (b). The detail scratching parameters was tabulated in Table 1.

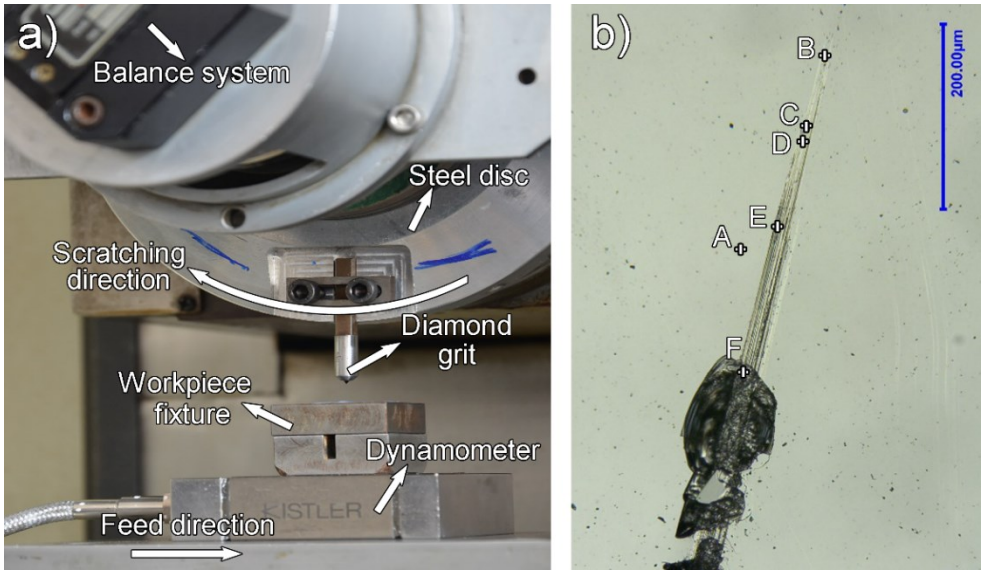

Fig. 1 (a) Experimental setup, and (b) a typical scratching groove

Nanoindentation test was conducted on a nano-indenter (Nano-Indenter® XP system, MTS) with a Berkovich indenter in continuous stiffness measurement (CSM) mode. To study the effects of the loading/unloading rate and the maximum load, nanoindentation tests were performed at two selected loading/unloading time (5 s and 20 s) and three maximum loads (10 mN, 50 mN and 100 mN). To make the results more reliable, three repeated imprints were conducted under each condition.

Table 1 Detail scratching parameters

Machine	MUGK7120X5
Grit shape	Face-to-face apex angle 120°
Scratching diameter	230 mm
Rotation speed	50 RPM
Feed rate	1000 mm/min

The surface topography of the diamond grit was characterized by an optical microscope (KEYENCE VHX-15), and the surface morphology of the indenter and the scratching groove was examined by a scanning electron microscope (SEM, JEOL Model JSM-6490) equipped with an energy disperse spectroscopy (EDS). Raman spectroscopy was carried out on an Xplora system (Horiba) at the room temperature. The wavelength of the laser used was 532 nm, with the test time of 10 s for each under the SWIFT Co-Focus imaging mode. An average intensity of two measurements was recorded, and the confocal imaging resolution reaches submicron range with the 100× objective lens. Varied points (Point B, C, D, E, F) along the scratching groove were examined, as well as the non-machined surface of about 50 μm next to the groove (Point A), which is indicated in Fig. 1 (b). The surface topography of the original Si workpiece

and the cross sectional profile of the scratching groove were examined by the Nexview three dimensional profiler (ZygoLamda).

RESULTS AND DISCUSSION

Fig. 2 (a) and (b) shows the surface topography and morphology of the diamond grit after the scratching test, which indicated that obvious wear appeared. The worn morphology of the diamond grits played a determinant role on the surface formation during the ultra-precision machining process, as it not only has a great impact on the scratching force, but also on the distribution of temperature. Actually, the cross sectional profile of the scratching groove was determined by the sharp edges distributed randomly on the worn diamond grit. The surface height profiles across the groove at varied positions (Position B, C, D, E), as indicated in Fig. 1 (b), are shown in Fig. 2 (c). At the beginning of the scratching groove (Position B), only ductile sliding traces was generated. With increasing depth of cut, more sharp edges on the worn indenter participated in ploughing, and an increasing depth of grooves (Position C and D) were induced by the diamond grit. At position E, the micro-broken occurred and the extrusion of Si was also produced at the side of the scratching groove.

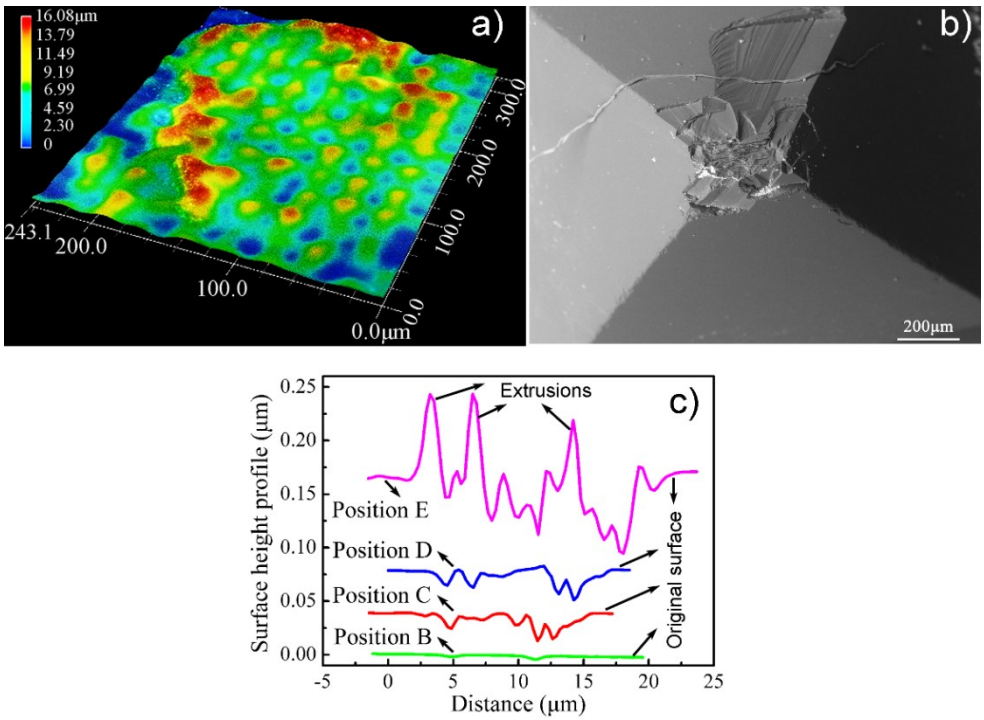

Fig. 2 (a) Surface topography and (b) surface morphology of the diamond indenter after scratching; (c) cross-sectional profiles of the scratched groove at different positions

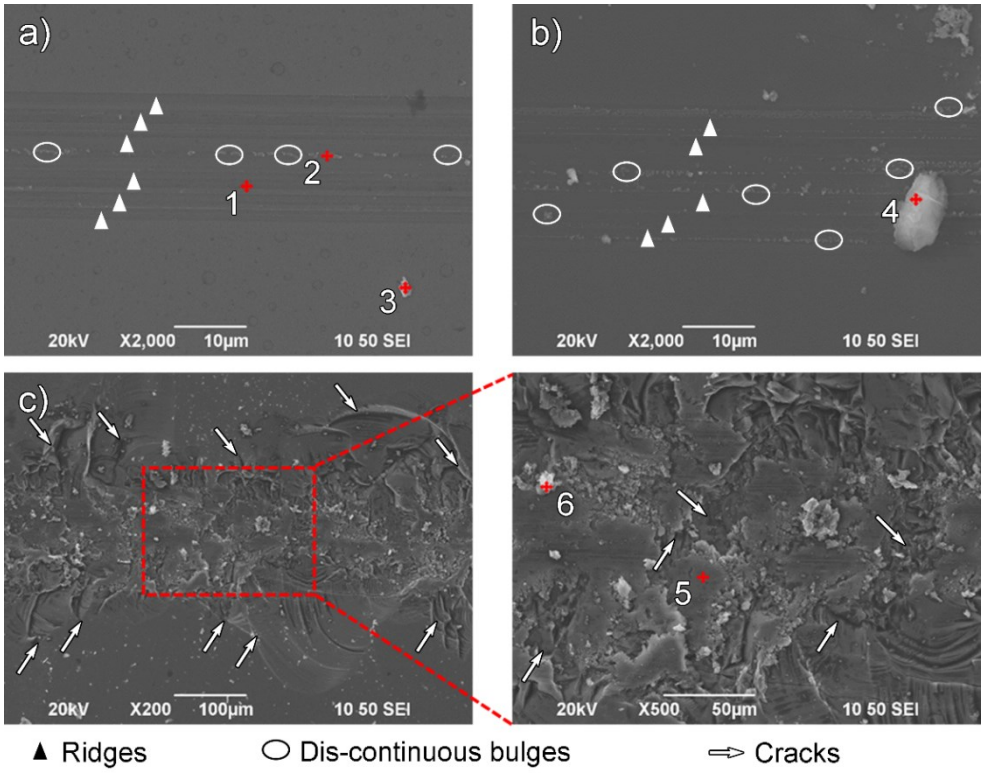

Fig. 3 Surface morphology of the scratched monocrystalline Si at different positions

To get a further insight into the surface damage mechanism, SEM images of the scratching groove at different positions is shown in Fig. 3. It could be easily found that only ductile scratched grooves were generated at the initial stage of the scratching, without obvious chips left on the workpiece surface. However, some micro-ridges and discontinuous bulges formed, which was attributed to the worn surface of the diamond indenter, as shown in Fig. 2. With the increase of the scratching depth, obvious chips formed and remained on the workpiece surface, and more discontinuous bulges was produced. As the cutting depth was greater than the critical depth of cut, cracking was induced, which prompted the bulk material removal, especially at the side points of the groove. As shown in Table 2, EDS results of the varied points in Fig. 3 (Points 1, 2, 3, 4, 5, 6) also indicate that not only the chemical reaction between the diamond indenter and Si could be induced under the high temperature, but also obvious oxidation of silicon appeared under dry scratching. In addition, it could be found that the chemical reaction between C and Si atoms occurred earlier than the oxidation during the scratching, which corresponded to the free energy change of these two reactions [28, 31]. The appearance of chemical reaction should also account for the serious diamond grits wear in combination with the high pressure induced fracture [32].

Table 2 Semi-quantitative EDS results for the points marked in Fig. 3

Points	Si	C	O
1	100	-	-
2	100	-	-
3	70.85	29.15	-
4	75.60	24.40	-
5	73.29	26.71	-
6	45.46	51.68	2.86

For studying the phase transformation of Si, previous investigations have proved Raman spectroscopy to be an effective method [8, 13, 15, 24]. The Raman wavenumber of single crystal Si is typically located at 521 cm^{-1}, while the broadening and low intensity peaks at 150 $cm^{-1}$and 470 cm^{-1} are representative for the amorphous Si [27, 33]. Fig. 4 shows the Raman spectra for the different points of the scratching groove. At the original surface (Point A) near the scratching grooves, a “triplet-peak” appeared for the Raman spectra, which indicates the complex strain state there. In addition, the chipping Si particles and finer grooves would also contribute to the formation of the “triplet-peak”. As has been proposed in Refs. [16] and [33], the down-shift of Raman band is attributed to the compression, while the up-shift can be caused by the tension. In addition, the small domain of crystalline could also result in the down-shift [34-36]. Point B at the ductile material removal region of the groove was also examined. Compared with that of point A, the Raman spectra intensity decreased obviously. With the further increase of scratching depth at point D, amorphization of the crystal Si occurred, for which the Raman spectra band become broader and shift to a lower wavenumber (498 cm^{-1}). The asymmetry of the spectra also indicates the existence of amorphous Si. At point E, the intensity further decreased and the peak shifted to be around 470 cm^{-1}, which indicated a thorough amorphization for the outmost layer. Thick amorphized layer was also identified for the scratching chips (Point C) and the peak intensity even disappeared in the wavenumber range.

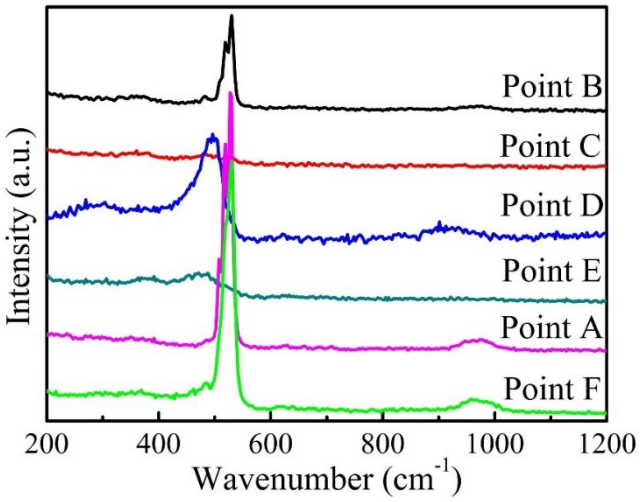

Fig. 4 Raman spectra of the varied points in the scratching groove

Great attention should also be paid to the surface fracture. At the fracture point (Point F), the dislodgement of metamorphic materials resulted in the disclosure of crystalline materials. Therefore, the peak wavenumber and intensity kept even the same with the original surface. Specifically, the peak intensity (at around 525 cm^{-1}) was almost the same with the original surface (Point A), but the separated peaks (510 cm^{-1}, 520 cm^{-1}, 530 cm^{-1}) became unclear. The crack induced stress relief should account for this phenomenon. Furthermore, there were no other evident polymorph peaks occurred for crystalline Si, such as Si-III (bc8) and Si-XII (r8) phases [37, 38]. It has been reported that the diamond cubic structure Si firstly transferred to β-Sn type Si (II) metallic structure under a high pressure [14, 19, 39]. However, the following transformation were dependent on the strain rate, where β-Sn structure Si (Si-II) transforms to amorphous Si directly at the rapid loading/unloading condition [2, 13]. In Ref. [30], the critical depth of cut d_e for monocrystalline Si was simulated to be ~387.6 nm, much larger than the present work (~60±15 nm, Point E). This was attributed to the Si-I to β-Sn structure Si (Si-II) and the following β-Sn structure Si (Si-II) to amorphous Si transformation under the rapid loading/unloading of the diamond grit. So the dramatic volume change also prompted the surface fracture.

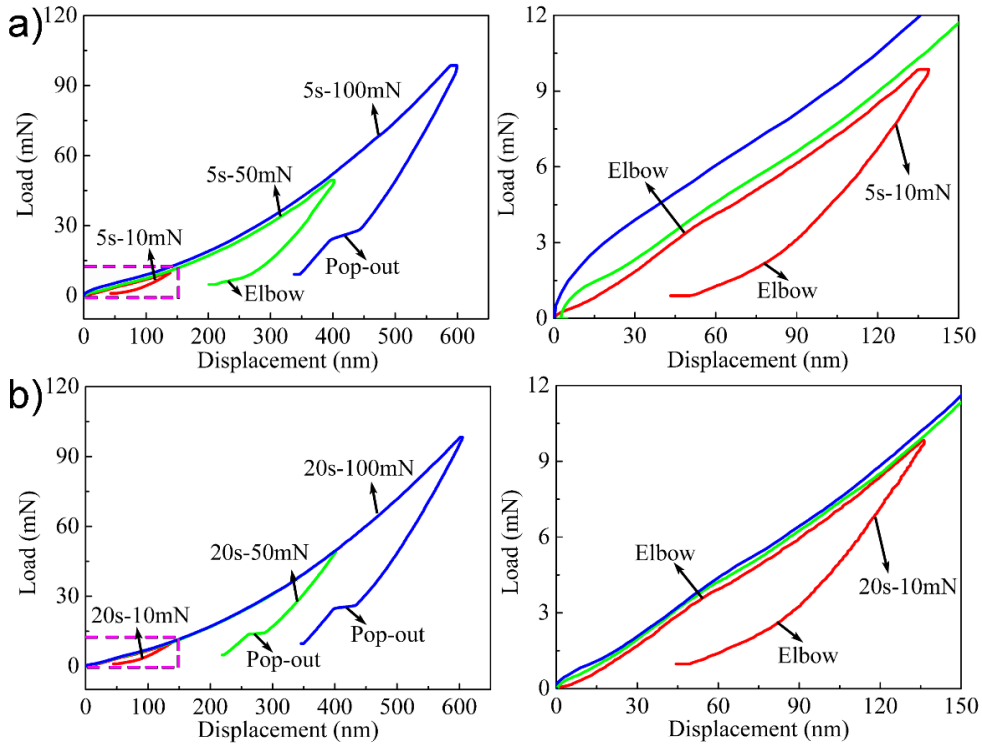

Fig. 5 (a) Load-displacement curves for Nano-indentation test at 5 s-10 mN, 5 s-50 mN and 5 s-100 mN and the enlarged view of the dashed box; (b) load-displacement curves for Nano-indentation test at 20 s-10 mN, 20 s-50 mN and 20 s-100 mN and the enlarged view of the dashed box

To further confirm the impact of the phase transformation, nanoindentation tests under the selected loading/unloading conditions were performed and the load-displacement curves are shown in Fig. 5. It can be easily seen that an elbow appears with the maximum load of 10 mN during the unloading stage. In addition, the unloading curve has an elbow and pop-out point at 5 s-50 mN and 5 s-100 mN, respectively, while the pop-out appeared for the loading/unloading condition of 20 s-50 mN and 20 s-100 mN. This is regarded as an indication of the polymorph transformation of Si [11, 15]. As was reported in Refs. [13] and [15], the higher loads and fast loading/unloading led to the appearance of pop-out in the unloading curve, while an elbow could be found at the slower rates and lower loads. The results presented in Fig. 5 corresponded with it. However, previous studies only focused on the abnormal curves during the unloading stage, and few research reported the phase transformation induced “elbow” curve during the loading period [11, 15, 40], which is identified in the present work. Specifically, during the initial loading stage, an elbow also occurred for each curve, which indicates the transformation of Si-I to β-Sn structure Si (Si-II). The high density of β-Sn structure Si (Si-II) resulted in a volume decrease (22%) [12, 13], and it contributed to the displacement, so the slope dropped after the elbow point. Under the greater loads and faster

loading/unloading rates, the larger plastic deformation and rapid volume increase (Si-II to a-Si) contributes to the crack formation near the imprint, as shown in Fig. 6. This further confirmed the results that phase transformation of Si during the rapid scratching can lead to the reduction of critical depth of cut.

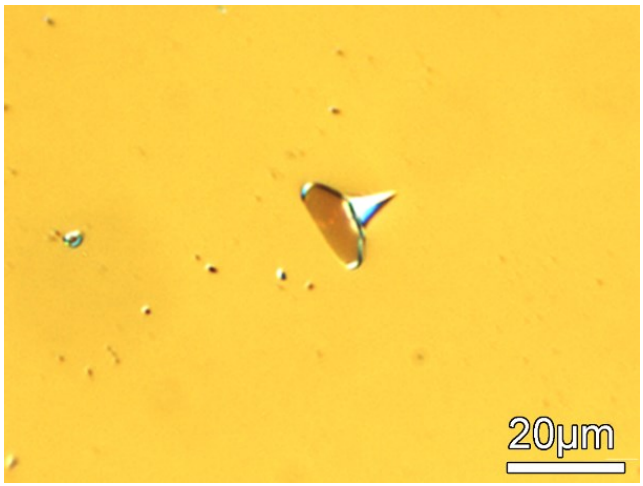

Fig. 6 Surface morphology of nanoindentation profile under 20 s-100 mN

CONCLUSIONS

In summary, the high pressure phase transformation of monocrystalline Si under indentation was dependent on the loading/unloading conditions. An 'Elbow' curve during the loading stage could also be induced by the phase transformation of Si, while the rapid loading/unloading could result in the amorphization of Si, and the phase transformation accompanied with the rapid volume change contributed to the surface fracture under the diamond scratching, where surface fracture occurred far below the critical depth of cut under the diamond scratching. In addition, chemical reaction between the worn diamond grit and Si and oxidation of Si were identified, which prompted the wear of diamond indenter. In addition, the cross sectional profile of the scratching groove was generated closely dependent on the worn surface of the diamond grit.

ACKNOWLEDGEMENT

The work was supported by the National Natural Science Foundation of China (NSFC) (Project No.:51475109) and also the Research Committee of the Hong Kong Polytechnic University (RTRA). In addition, we would like to show great thanks for the kindly help from Mr. Mingtao Wu.

REFERENCES

[1]. H.K. Tönshoff, W. V. Schmieden, I. Inasaki, W. König, and G. Spur, CIRP Ann. - Manuf. Technol. 39, 621 (1990).

[2]. I. Zarudi, J. Zou, W. McBride, and L.C. Zhang, Appl. Phys. Lett. 85, 932 (2004).

[3]. I. Zarudi, T. Nguyen, and L.C. Zhang, Appl. Phys. Lett. 86, 011922 (2005).

[4]. J. Yan, J. Appl. Phys. 95, 2094 (2004).

[5]. H. Shin, B. Kim, J. Kim, S. Hwang, A.S. Budiman, H. Son, K. Byun, N. Tamura, M. Kunz, D. Kim, and Y. Joo, J. Electron. Mater. 41, 712 (2012).

[6]. A.S. Budiman, G. Illya, V. Handara, W.A. Caldwell, C. Bonelli, M. Kunz, N. Tamura, and D. Verstraeten, Sol. Energy Mater. Sol. Cells 130, 303 (2014).

[7]. S.K. Tippabhotla, I. Radchenko, K.N. Rengarajan, G. Illya, V. Handara, M. Kunz, N. Tamura, and A.S. Budiman, Procedia Eng. 139, 123 (2016).

[8]. Y.G. Gogotsi, V. Domnich, S.N. Dub, A. Kailer, and K.G. Nickel, J. Mater. Res. 15, 871 (2000).

[9]. U. Schwarz, K. Syassen, K. Takemura, and M. Hanfland, Phys. Rev. Lett. 82, 1197 (1999).

[10]. M.C. Kroll, P.D. Kirchner, R.F. Cook, B.J. Hockey, and D.R. Clarke, Phys. Rev. Lett. 60, 2156 (1988).

[11]. H. Huang and J. Yan, Scripta Mater. 102, 35 (2015).

[12]. D.E. Kim and S.I. Oh, Nanotechnology 17, 2259 (2006).

[13]. A. Kailer, Y.G. Gogotsi, and K.G. Nickel, J. Appl. Phys. 81, 3057 (1997).

[14]. K. Gaál-Nagy, M. Schmitt, P. Pavone, and D. Strauch, Comp. Mater. Sci. 22, 49 (2001).

[15]. V. Domnich, Y. Gogotsi, and S. Dub, Appl. Phys. Lett. 76, 2214 (2000).

[16]. B.V. Tanikella, A.H. Somasekhar, A.T. Sowers, R.J. Nemanich, and R.O. Scattergood, Appl. Phys. Lett. 69, 2870 (1996).

[17]. T. Tian, R. Morusupalli, H. Shin, H.Y. Son, K.Y. Byun, Y.C. Joo, R. Caramto, L. Smith, Y. Shen, M. Kunz, N. Tamura, and A.S. Budiman, Procedia Eng. 139, 101 (2016).

[18]. K.N. Rengarajan, I. Radchenko, G. Illya, V. Handara, M. Kunz, N. Tamura, and A.S. Budiman, Procedia Eng. 139, 76 (2016).

[19]. J. Sun, L. Fang, J. Han, Y. Han, H. Chen, and K. Sun, Comp. Mater. Sci. 82, 140 (2014).

[20]. Y. Wang, J. Zou, H. Huang, L. Zhou, B.L. Wang, and Y.Q. Wu, Nanotechnology 18, 465705 (2007).

[21]. T.F. Page, W.C. Oliver, and C.J. McHargue, J. Mater. Res. 7, 450 (1992).

[22]. J. Yan, H. Takahashi, J.I. Tamaki, X. Gai, H. Harada, and J. Patten, Appl. Phys. Lett. 86, 181913 (2005).

[23]. T. Shibata, S. Fujii, E. Makino, and M. Ikeda, Precis. Eng. 18, 129 (1996).

[24]. J. Yan, T. Asami, H. Harada, and T. Kuriyagawa, Precis. Eng. 33, 378 (2009).

[25]. A.S. Budiman, K.R. Narayanan, N. Li, J. Wang, N. Tamura, M. Kunz, and A. Misra, Mater. Sci. Eng. A 635, 6 (2015).

[26]. A.S. Budiman, S. Han, N. Li, Q. Wei, P. Dickerson, N. Tamura, M. Kunz, and A. Misra, J. Mater. Res. 27, 599 (2012).

[27]. J. Yan, T. Asami, and T. Kuriyagawa, Precis. Eng. 32, 186 (2008).

[28]. S. Goel, X. Luo, and R.L. Reuben, Tribol. Int. 57, 272 (2013).

[29]. Q. Zhang, S. To, Q. Zhao, and B. Guo, Mater. Lett. 172, 48 (2016).

[30]. H. Wu and S.N. Melkote, J. Eng. Mater. Technol.-T. ASME 134, 41011 (2012).

[31]. Z. Cheng, MSc Thesis-Materials Science and Engineering, Georgia Institute of Technology, 2004.

[32]. W.J. Zong, T. Sun, D. Li, K. Cheng, and Y.C. Liang, Int. J. Mach. Tools Manu. 48, 1678 (2008).

[33]. Y. Gogotsi, C. Baek, and F. Kirscht, Semicond. Sci. Technol. 14, 936 (1999).

[34]. J. Zi, H. Büscher, C. Falter, W. Ludwig, K. Zhang, and X. Xie, Appl. Phys. Lett. 69, 200 (1996).

[35]. G. Viera, S. Huet, and L. Boufendi, J. Appl. Phys. 90, 4175 (2001).

[36]. I.H. Campbell and P.M. Fauchet, Solid State Commun. 58, 739 (1986).

[37]. J.R. Maclean, S.J. Clark, G.J. Ackland, P.D. Hatton, J. Crain, and R.O. Piltz, Phys. Rev. B 52, 4072 (1995).

[38]. S.A. Solin, M. Selders, R.K. Chang, R. Alben, M.F. Thorpe, D. Weaire, and R.J. Kobliska, Phys. Rev. Lett. 29, 725 (1972).

[39]. X. Li, J. Lu, B. Liu, and S. Yang, Tribol. Int. 41, 189 (2008).

[40]. H. Huang and J. Yan, Semicond. Sci. Technol. 30, 115001 (2015).

Figure captions:

Fig. 1 (a) Experimental setup, and (b) a typical scratching groove

Fig. 2 (a) Surface topography and (b) surface morphology of the diamond indenter after scratching; (c) cross-sectional profiles of the scratched groove at different positions

Fig. 3 Surface morphology of the scratched monocrystalline Si at different positions

Fig. 4 Raman spectra of the varied points in the scratching groove

Fig. 5 (a) Load-displacement curves for Nano-indentation test at 5 s-10 mN, 5 s-50 mN and 5 s-100 mN and the enlarged view of the dashed box; (b) load-displacement curves for Nano-indentation test at 20 s-10 mN, 20 s-50 mN and 20 s-100 mN and the enlarged view of the dashed box

Fig.6 Surface morphology of nanoindentation profile under 20 s-100 mN